Stem Cell Reports
Article

ISSCR

OPEN ACCESS

Cell-Based Delivery of Interleukin-13 Directs Alternative Activation of Macrophages Resulting in Improved Functional Outcome after Spinal Cord Injury

Dearbhaile Dooley,[1,2] Evi Lemmens,[1] Tim Vangansewinkel,[1] Debbie Le Blon,[2] Chloé Hoornaert,[2] Peter Ponsaerts,[2,3] and Sven Hendrix[1,3,*]

[1]Department of Morphology, Biomedical Research Institute, Hasselt University, Martelarenlaan 42, 3500 Hasselt, Belgium
[2]Laboratory of Experimental Hematology, Vaccine and Infectious Disease Institute (Vaxinfectio), University of Antwerp, Wilrijk, 2610 Antwerp, Belgium
[3]Co-senior author
*Correspondence: sven.hendrix@uhasselt.be
http://dx.doi.org/10.1016/j.stemcr.2016.11.005

SUMMARY

The therapeutic effects of mesenchymal stem cell (MSC) transplantation following spinal cord injury (SCI) to date have been limited. Therefore, we aimed to enhance the immunomodulatory properties of MSCs via continuous secretion of the anti-inflammatory cytokine interleukin-13 (IL-13). By using MSCs as carriers of IL-13 (MSC/IL-13), we investigated their therapeutic potential, compared with non-engineered MSCs, in a mouse model of SCI. We show that transplanted MSC/IL-13 significantly improve functional recovery following SCI, and also decrease lesion size and demyelinated area by more than 40%. Further histological analyses in $CX_3CR1^{EGFP/+}$ $CCR2^{RFP/+}$ transgenic mice indicated that MSC/IL-13 significantly decrease the number of resident microglia and increase the number of alternatively activated macrophages. In addition, the number of macrophage-axon contacts in MSC/IL-13-treated mice was decreased by 50%, suggesting a reduction in axonal dieback. Our data provide evidence that transplantation of MSC/IL-13 leads to improved functional and histopathological recovery in a mouse model of SCI.

INTRODUCTION

Stem cell therapies for CNS injury have raised a lot of hope among patients, doctors, and scientists in recent years. Although we are still in the early stages of developing successful approaches in humans, numerous preclinical animal studies support the therapeutic ability of stem cells (Martino and Pluchino, 2006; Orlacchio et al., 2010; Urdzíková et al., 2014). Despite these observations, the dual role of the neuroinflammatory response following CNS injury makes stem cell-supported regeneration difficult due to the presence of inhibitory immune factors that are upregulated in and around the lesion site. Therefore, modulating the inflammatory milieu by upregulating anti-inflammatory cytokines may be crucial when designing therapies for CNS repair (Dooley et al., 2013). With this in mind, using mesenchymal stem cells (MSCs) as an immune-modulating cellular therapy may exert positive effects in rodent models of spinal cord injury (SCI) (Alexanian et al., 2011; Nakajima et al., 2012). Here, we test the hypothesis that using MSCs as carriers for the delivery of the canonical anti-inflammatory cytokine interleukin-13 (IL-13) may further enhance their therapeutic potential.

Despite much debate regarding the detrimental effects of CNS inflammation, many studies have also outlined its significance in tissue repair, including a therapeutic potential of microglia/macrophages in promoting axonal regeneration (Hendrix and Nitsch, 2007; Rolls et al., 2009). Almost all tissues contain several types of phagocytic cell populations, consisting of macrophages and/or microglia, which have specialized functions and distinct phenotypic properties (Boyle et al., 2003; Protzer et al., 2012). A rather simplistic but pragmatic way to distinguish the varying microglia/macrophage subsets is to divide them into classically (M1) or alternatively activated (M2) phenotypes (Bogie et al., 2014; Gordon, 2003). M2 microglia/macrophages differentiate from the classically activated M1 microglia/macrophages and are less inflammatory in nature. They are characterized by a reduced nitric oxide production and less secretion of proinflammatory cytokines (Bruce-Keller et al., 2001). They also express markers such as arginase-1 (ARG-1) and *Found in inflammatory zone 1* (FIZZ1), which differentiate them from classically activated M1 microglia/macrophages (Colton, 2009). However, a more specific characterization indicates that upregulation of major histocompatibility complex II (MHC-II) (in both M1 and M2 cell subsets) is associated with macrophage activation. It is currently suggested that the joint expression of MHC-II and ARG-1/FIZZ1 is indicative of a neuroprotective and anti-inflammatory, M2a phenotype (Mantovani et al., 2004); however, the exact mode of action of this polarized cell type has not yet been unraveled. Nevertheless, reducing the proinflammatory M1 phenotype upon CNS

injury in favor of the beneficial M2a phenotype is of particular therapeutic interest.

This polarizing approach toward an M2a phenotype may be of great therapeutic value, particularly following SCI. After injury, infiltration of axon-attacking macrophages greatly contributes to axonal retraction and the deleterious phenomenon known as axonal dieback (Busch et al., 2009; Horn et al., 2008). This leads to exacerbation of damage and increased functional deficits. Therefore, in this study we aimed to target these macrophages and drive them toward a less destructive phenotype to limit axonal dieback and improve functional recovery. To do this, we chose to use the immunomodulatory cytokine, IL-13, which is a well-known inducer of the M2a microglia/macrophage phenotype (Doherty et al., 1993; Doyle et al., 1994). IL-13 has also been shown to exert neuroprotective effects in the experimental autoimmune encephalomyelitis model of multiple sclerosis, by decreasing inflammatory cell infiltration and axonal loss as well as reducing clinical symptoms (Cash et al., 1994; Ochoa-Repáraz et al., 2008; Offner et al., 2005). We recently demonstrated that after SCI in mice, IL-13 levels decrease significantly in the spinal cord within hours after injury (Nelissen et al., 2013). Therefore, given the drop in IL-13 levels after injury and its polarizing capabilities toward a more neuroprotective M2 macrophage phenotype, it is plausible that application of IL-13 in the acute phase after SCI may have therapeutic potential.

To efficiently deliver IL-13 to the injured spinal cord, we used autologous MSCs genetically engineered to secrete IL-13. We hypothesized that this enhanced cellular therapy is capable of modulating the microglia/macrophage response and improving functional recovery after SCI. To support our hypothesis, we investigated the effects of grafting control MSCs and those expressing IL-13 (MSC/IL-13) in a mouse model of SCI. We show that transplantation of MSCs which continuously secrete IL-13 significantly improves functional recovery and decreases both lesion size and demyelinated area after SCI. Finally, we propose a mode of action in which delivery of IL-13 from MSC grafts to the injured spinal cord polarizes macrophages to a neuroprotective M2a phenotype, subsequently reducing the number of axon-attacking macrophages and improving functional outcome.

RESULTS

Transplantation of MSC/IL-13 Improves Functional Recovery and Reduces Lesion Size and Demyelinated Area

In the first part of this study, we investigated whether MSCs genetically engineered to express IL-13 could improve functional recovery following SCI in BALB/c and C57BL/6 mice. Mice were treated with either vehicle (NaCl), control MSCs (MSC), or IL-13-secreting MSCs (MSC/IL-13) immediately after SCI and functional recovery was measured 4 weeks post injury using the Basso Mouse Scale (BMS). In BALB/c mice, both MSC- and MSC/IL-13-treated animals displayed a significantly improved functional recovery compared with NaCl controls (Figure 1A). Lesion size quantification revealed a significant decrease in mice receiving transplantation of MSC/IL-13 compared with control MSCs and NaCl (Figure 1B). Similarly, demyelinated area was significantly decreased in MSC/IL-13-treated mice compared with control MSC and NaCl (Figure 1C). In contrast to BALB/c mice, treatment with MSC/IL-13 in C57BL/6 mice significantly improved functional recovery compared with control MSCs or NaCl (Figure 1D). Additionally there was a corresponding significant decrease in both lesion size (Figure 1E) and demyelinated area (Figure 1F) in MSC/IL-13 compared with control MSCs or NaCl. In both mouse backgrounds, immunofluorescence stainings for glial fibrillary acidic protein (GFAP) (Figures 1G–1I) and myelin basic protein (MBP) (Figures 1J–1L) were used to analyze lesion size and demyelinated area, respectively. Taken together, these data demonstrate that on a functional level, BALB/c mice can benefit from both MSC and MSC/IL-13 grafts, while C57BL/6 mice require MSC/IL-13 grafts for improved outcome. However, on the histopathological level, both BALB/c and C57BL/6 mice benefit from MSC/IL-13 grafts to reduce lesion size and demyelination.

MSC/IL-13 Transplantation Has No Significant Effect on the Presence of Microglia/Macrophages at the Lesion Site in Both BALB/c and C57BL/6 Mice, but Leads to a Significant Reduction in Astrogliosis in C57BL/6 Mice

In a first attempt to understand why MSC/IL-13, but not MSC grafts, reduce lesion size and demyelination, we investigated the degree of microglia/macrophage (Figures 2A and 2I) and astroglial (Figures 2B and 2J) responses in both BALB/c and C57BL/6 mice at 4 weeks post injury. For analysis, quantification of IBA-1 (Figures 2C–2E and 2K–2M) and GFAP (Figures 2F–2H and 2N–2P) intensity was performed 600 μm caudal and 600 μm rostral from the lesion site, in squares measuring 100 × 100 μm in BALB/c and C57BL/6 mice, respectively. There was no significant difference observed in the presence of microglia/macrophages in mice treated with MSC or MSC/IL-13 compared with NaCl controls in both BALB/c and C57BL/6 mouse backgrounds (Figures 2A and 2I, respectively). In addition, there was

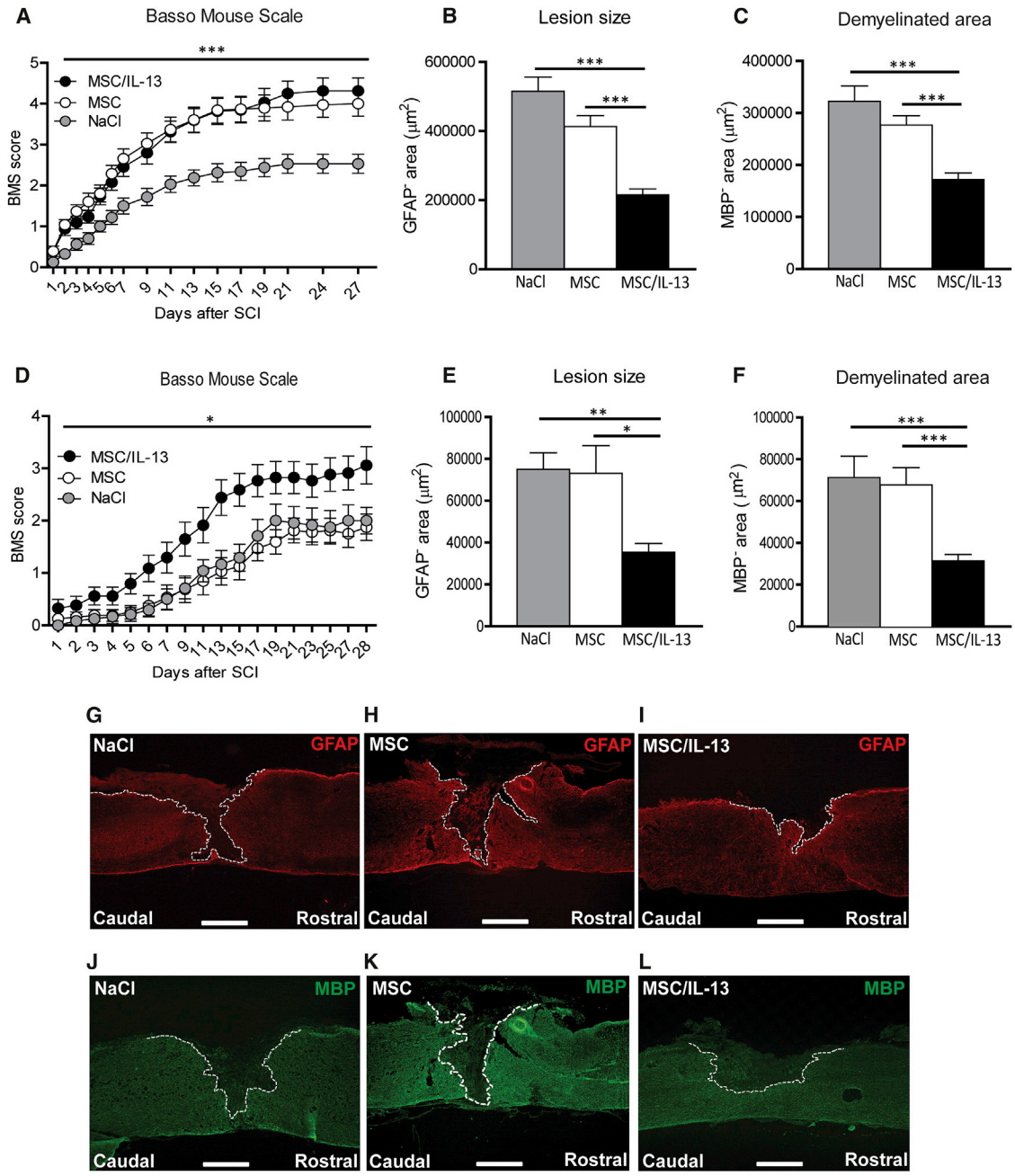

Figure 1. Transplantation of MSC/IL-13 Improves Functional Recovery and Reduces Lesion Size and Demyelinated Area in Mice Following SCI

(A–C) BALB/c mice receiving transplantation of MSCs or MSC/IL-13 show a significantly increased BMS score following SCI (A). ***$p < 0.0001$, n = 16–19/group. Image analysis revealed a significant decrease in (B) lesion size and (C) demyelinated area in the MSC/IL-13-treated animals, compared with MSC and NaCl groups. ***$p < 0.0001$, n = 6–8/group.

(D–L) C57BL/6 mice receiving transplantation of MSC/IL-13 show a significantly increased BMS score following SCI, compared with MSC or NaCl controls (D). *$p < 0.05$, n = 12–17/group. Image analysis for GFAP and MBP staining also revealed a significant decrease in (E) lesion size and (F) demyelinated area, respectively, in MSC/IL-13-treated animals, compared with MSC and NaCl controls. Data represent mean ± SEM. ***$p < 0.0001$, **$p < 0.01$, *$p < 0.05$; n = 8–10/group. Representative photomicrographs are shown of BALB/c spinal cord sections including the injury epicenter of MSC (G, J), NaCl-treated MSC (H, K), and (I, L) MCS/IL-13-treated mice. Sections were stained for (G–I) GFAP and (J–L) MBP to determine the lesion size and demyelinated area as depicted by the dotted white line. Scale bars in (G) to (L) represent 500 μm.

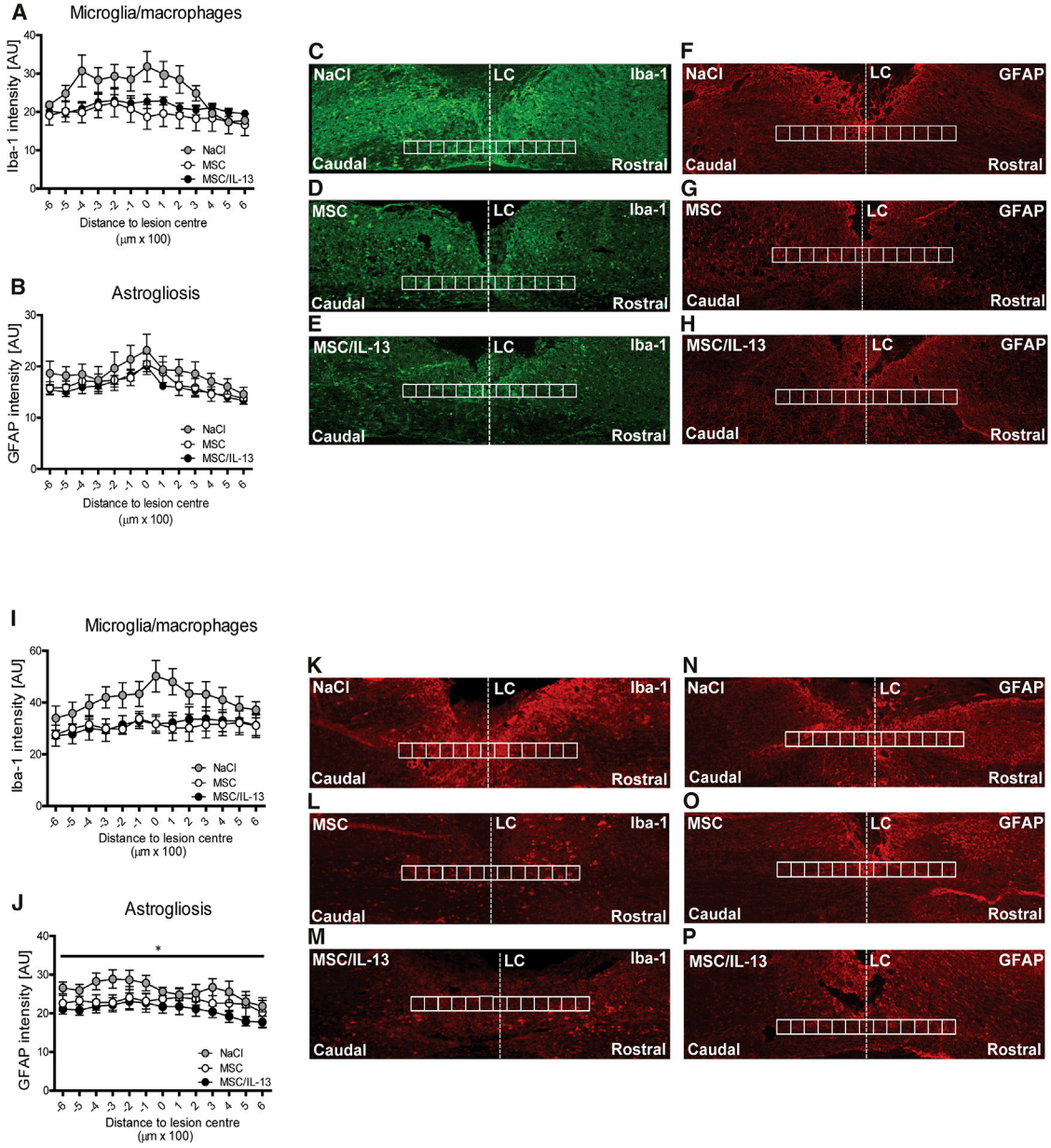

Figure 2. MSC/IL-13 Transplantation Has No Significant Effect on the Presence of Microglia/Macrophages at the Lesion Site in Both BALB/c and C57BL/6 Mice, but Leads to a Significant Reduction in Astrogliosis in C57BL/6 Mice

In BALB/c mice, there was no significant difference observed in the presence of (A) microglia/macrophages or (B) astrogliosis in (C and F) NaCl-treated, (D and G) MSC-treated, or (E and H) MSC/IL-13-treated animals as measured via intensity analysis for IBA-1 and GFAP, respectively. In C57BL/6 mice, there was no significant difference observed in the presence of (I) microglia/macrophages in (K) NaCl-treated, (L) MSC-treated, or (M) MSC/IL-13-treated animals. However, quantification of GFAP in C57BL/6 mice revealed a significant decrease in (J) astrogliosis in mice treated with (P) MSC/IL-13- compared with (O) MSC- or (N) NaCl-treated mice. All analyses (C–H, K–P) were quantified within square areas of 100 × 100 μm just below the lesion site, extending 600 μm rostral to 600 μm caudal from the lesion epicenter. Data represent mean ± SEM. *$p < 0.05$; n = 7–11/group.

no significant difference in astrogliosis in MSC- or MSC/IL-13-treated mice compared with NaCl controls in BALB/c mice (Figure 2B). However, there was a significant reduction in astrogliosis in C57BL/6 mice treated with MSC/IL-13 when compared with MSC on NaCl controls (Figure 2J).

Transplantation of MSC/IL-13 Increases the Number of Neuroprotective, Alternatively Activated Macrophages at the Graft Site and Increases the Number of CD4$^+$ T Cells throughout the Spinal Cord

To further investigate the effects of MSC/IL-13 grafting, we characterized the classically activated and alternatively activated microglia/macrophage phenotypes at the level of the graft site (Figure 3A-ii) by performing an intensity analysis for MHC-II and ARG-1, respectively. While there was no difference in MHC-II intensity between the MSC and MSC/IL-13 graft (Figures 3B, 3D, and 3F), there was a significant increase in ARG-1 intensity within the MSC/IL-13 graft region compared with that of the MSC graft (Figures 3G, 3I, and 3K). The graft site regions of interest (ROIs) analyzed using MHC-II and ARG-1 intensity analysis are shown in Figures 3C and 3E (white box) and Figures 3H and 3J, respectively. The ROIs in Figures 3C and 3E are shown at a higher magnification in Figures 3D and 3F, and the ROIs in Figures 3H and 3J are shown in Figures 3I and 3K. These data strongly suggest that the secretion of IL-13 from MSC grafts significantly increases the presence of an alternatively activated microglia/macrophage phenotype at the graft site. Quantification of CD4$^+$ T cells throughout the spinal cord revealed a significant increase in the number of CD4$^+$ T cells in MSC/IL-13-treated mice compared with MSC- and NaCl-treated controls in both BALB/c (Figures 3L–3O) and C57BL/6 Figures 3P–3S) mouse backgrounds.

Transplantation of MSC/IL-13 Increases the Number of Neuroprotective, Alternatively Activated Macrophages and Decreases the Number of Microglia at the Graft Site

The data provided above demonstrate that MSC/IL-13 grafts significantly increase the presence of alternatively activated microglia/macrophage phenotypes at the level of the graft site. However, to investigate which of the two cell types (microglia or macrophages) was responsible for the increase in ARG-1 expression, we took advantage of the C57BL/6 $CX_3CR1^{EGFP/+}$ $CCR2^{RFP/+}$ mouse model. This model allows us to distinguish between EGFP$^+$RFP$^-$ microglia (green) as well as EGFP$^-$RFP$^+$ macrophages (red) and EGFP$^+$RFP$^+$ macrophages (yellow) as outlined in Experimental Procedures. Following SCI, we grafted MSC or MSC/IL-13 and investigated the graft immune response by performing immunofluorescence staining for MHC-II and ARG-1. We then calculated the cell density of microglia and macrophages at the graft site. Although there was no significant difference observed in the total microglia/macrophage cell density when comparing MSC and MSC/IL-13 grafts (Figure 4A), there was a clear difference in the origin and phenotype of infiltrating immune cells in MSC/IL-13 grafts compared with those in MSC grafts. Further quantification revealed a significant increase in the number of EGFP$^-$RFP$^+$ macrophages and a significant decrease in the number of EGFP$^+$RFP$^-$ microglia in MSC/IL-13-treated compared with control MSCs. There was no significant difference in the number of EGFP$^+$RFP$^+$ graft-infiltrating macrophages between MSC and MSC/IL-13 grafts (Figures 4B and 4C–4H). Based on these cell-density calculations, the proportion of MHC-II$^+$- or ARG-1$^+$-expressing cells within the EGFP$^-$RFP$^+$ and EGFP$^+$RFP$^+$ macrophage population, as well as within the EGFP$^+$RFP$^-$ microglia population, was calculated as outlined in Experimental Procedures (Figures 4I and 4P, respectively). For MHC-II expression (Figures 4I–4M), there was a significant increase in the number of MHC-II$^-$ and MHC-II$^+$ EGFP$^-$RFP$^+$ macrophages at the graft site in MSC/IL-13-treated mice compared with control MSCs. The proportion of MHC-II$^-$ and MHC-II$^+$ EGFP$^+$RFP$^+$ macrophages at the graft site was unaltered between MSC and MSC/IL-13 grafts. In contrast, we noted a significant reduction in MHC-II$^-$ EGFP$^+$RFP$^-$ microglia at the MSC/IL-13 graft site compared with the MSC graft, while the low number of MHC-II$^+$ EGFP$^+$RFP$^-$ microglia remained unaltered. This relative distribution of MHC-II expression within microglia and macrophage populations in MSC and MSC/IL-13 grafts is also represented in the corresponding pie charts (Figures 4N and 4O). When comparing ARG-1 expression between MSC and MSC/IL-13 grafts (Figures 4P–4T), there was a significant increase in the ARG-1$^+$ EGFP$^-$RFP$^+$ and EGFP$^+$RFP$^+$ macrophage populations, as well as the EGFP$^+$RFP$^-$ microglia population, in the MSC/IL-13-treated mice. Subsequently, there was a significant decrease in the ARG-1$^-$ EGFP$^+$RFP$^+$ macrophage population and ARG-1$^-$ EGFP$^+$RFP$^-$ microglia population, while the low amount of ARG-1$^-$ EGFP$^-$RFP$^+$ macrophages remained unchanged. The distribution of ARG-1 expression within microglia and macrophage populations in MSC and MSC/IL-13 grafts is also represented in the corresponding pie charts (Figures 4U and 4V). In summary, these results indicate that the number of macrophages is significantly higher and the number of microglia is significantly lower at the MSC/IL-13 graft site compared with control MSC grafts. Of the total macrophage populations present in MSC/IL-13 grafts, 30% express MHC-II (Figure 4O) while 53% express ARG-1 (Figure 4V, purple and white segments). Of the microglia present in MSC/IL-13 grafts, 5% express MHC-II (Figure 4O) while 15% express ARG-1 (Figure 4V, gray segments). Taken together, we demonstrate that there is a 10% increase in the number of MHC-II$^+$ immune cells and a 50% increase in the number of ARG-1$^+$ immune cells at the MSC/IL-13 graft site compared with control MSC grafts. These results indicate that the secretion of IL-13 from MSC grafts induces a broad spectrum of alternatively activated infiltrating macrophages at the graft site.

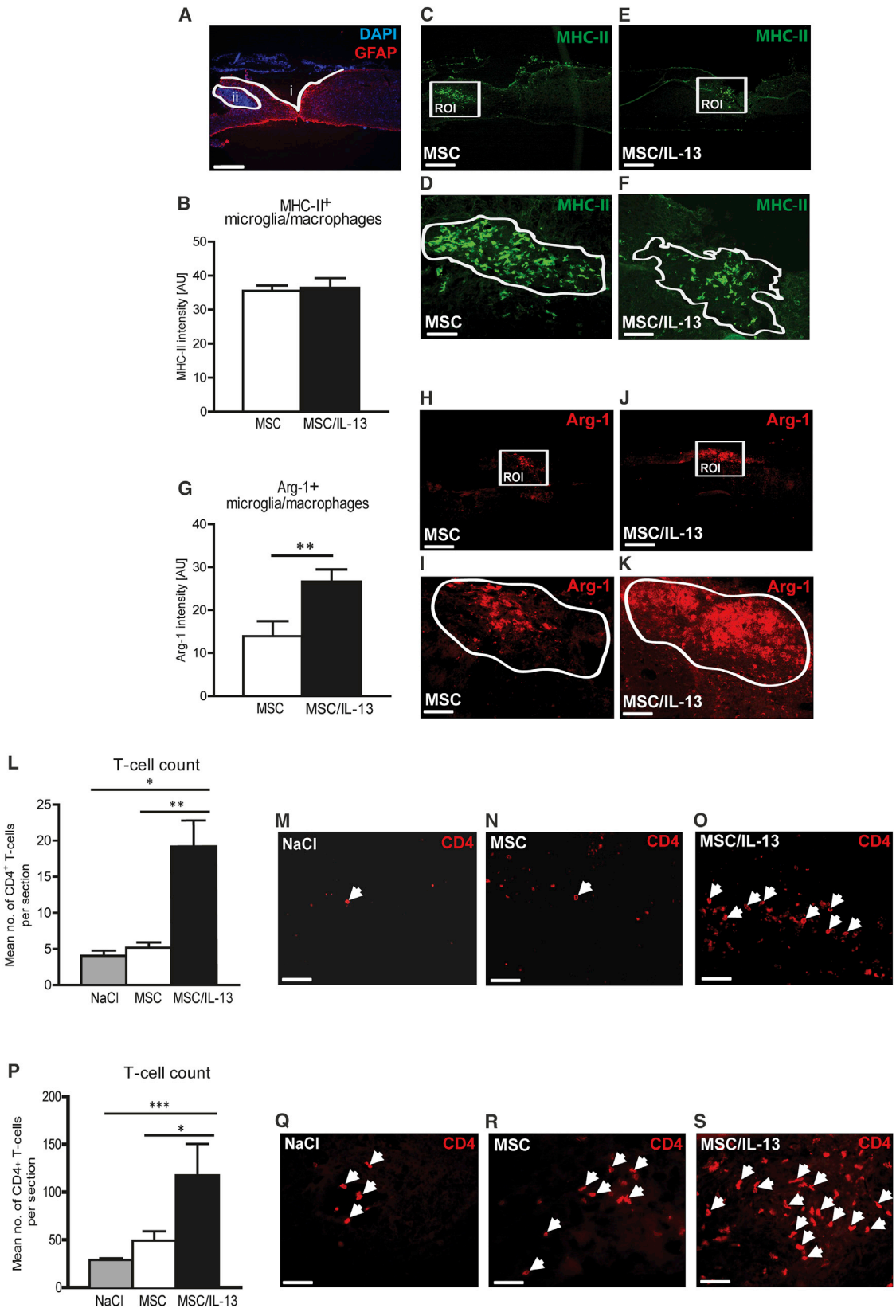

(legend on next page)

Transplantation of MSC/IL-13 Increases the Number of Infiltrating Neuroprotective, Alternatively Activated Macrophages and Decreases the Number of Microglia at the Lesion Site

Although analysis on the effects of IL-13 at the MSC graft site showed an increase in the number of neuroprotective, alternatively activated macrophages present, we hypothesized that a shift in the microglia/macrophage response at the spinal cord lesion site may also be possible, given the strong clinical benefit observed in MSC/IL-13-treated mice. Therefore, we also investigated the parameters described above at the lesion site in $CX_3CR1^{EGFP/+}$ $CCR2^{RFP/+}$ mice receiving MSC or MSC/IL-13 following SCI. Cell-density quantification at the lesion site revealed a significant increase in the total number of microglia/macrophages in mice treated with MSC/IL-13 compared with control MSCs (Figure 5A). More specifically, there was a significant increase in the number of $EGFP^-/RFP^+$ macrophages (red) and $EGFP^+/RFP^+$ macrophages (yellow), while the number of $EGFP^+/RFP^-$ microglia (green) was significantly decreased, in MSC/IL-13-treated compared with control MSC-treated mice (Figures 5B and 5C–5H). Similarly to the method described above at the graft site, we also calculated the proportion of MHC-II$^+$- or ARG-1$^+$-expressing microglia and macrophages at the lesion site. For MHC-II expression (Figures 5I–5M), there was a significant increase in the numbers of MHC-II$^-$ and MHC-II$^+$ $EGFP^-RFP^+$ macrophages at the lesion site in MSC/IL-13-treated mice compared with control MSCs. The proportion of MHC-II$^-$ $EGFP^+RFP^+$ macrophages at the lesion site was unaltered between MSC and MSC/IL-13 grafts, while the number of MHC-II$^+$ $EGFP^+RFP^+$ macrophages at the lesion site was significantly increased following MSC/IL-13 grafting. In contrast, we noted a significant reduction compared with control MSCs in MHC-II$^-$ $EGFP^+RFP^-$ microglia at the lesion site following MSC/IL-13 grafting, while the number of MHC-II$^+$ $EGFP^+RFP^-$ microglia remained unchanged. This relative distribution of MHC-II expression within microglia and macrophage populations at the lesion site following MSC and MSC/IL-13 grafting is also represented in the corresponding pie charts (Figures 5N and 5O). When comparing ARG-1 expression at the lesion site following MSC and MSC/IL-13 grafting (Figures 5P–5T), there was a significant increase in ARG-1$^+$ $EGFP^-RFP^+$ and $EGFP^+RFP^+$ macrophage populations, as well as the $EGFP^+RFP^-$ microglia population, in MSC/IL-13-treated mice. Subsequently, there was a significant decrease in the ARG-1$^-$ $EGFP^+RFP^-$ microglia population, while ARG-1$^-$ $EGFP^-RFP^+$ and ARG-1$^-$ $EGFP^+RFP^+$ macrophage populations remained unaltered. This relative distribution of ARG-1 expression within microglia and macrophage populations at the lesion site following MSC and MSC/IL-13 grafting is also represented in the corresponding pie charts (Figures 5U and 5V). These results indicate that similarly to the graft site, the number of macrophages is significantly higher and the number of microglia is significantly lower at the lesion site following MSC/IL-13 grafting compared with control MSCs. Of the macrophage populations present at the lesion site following MSC/IL-13 grafting, 36% express MHC-II (Figure 5O) while 67% express ARG-1 (Figure 5V, purple and white segments). Of the microglia present at the lesion site following MSC/IL-13 grafting, 11% express MHC-II (Figure 5O) while 8% express ARG-1 (Figure 5V, gray segments). This demonstrates that there is a 24% increase in the number of MHC-II$^+$ immune cells and a 60% increase in the number of ARG-1$^+$ immune cells at the lesion site following MSC/IL-13 grafting compared with control MSCs. Taken together, these results indicate that the secretion of IL-13 from MSC grafts (and/or the presence of alternatively activated microglia/macrophages at the MSC/IL-13 graft site) leads to an increased infiltration of peripheral

Figure 3. Transplantation of MSC/IL-13 Increases the Number of Neuroprotective, Alternatively Activated Macrophages at the Graft Site and Increases the Number of CD4$^+$ T Cells throughout the Spinal Cord

(A–K) To identify the lesion and graft site regions of interest (ROIs), we have included an overview of an SCI section (A) stained with GFAP + DAPI containing the (i) V-shaped lesion site and (ii) DAPI$^+$ intense MSC graft site encapsulated by GFAP$^+$ astrocytes. To determine the presence of (B) classically activated and (G) alternatively activated microglia/macrophages, we stained sections for (C–F) MHC-II or (H–K) ARG-1, respectively. (B) There was no significant difference in MHC-II levels between MSC and MSC/IL-13 graft regions. (G) There was a significant increase in ARG-1 levels within the MSC/IL-13 graft region compared with the MSC graft. Representative photomicrographs indicating the graft locations in (C and E) MHC-II and (H and J) ARG-1 stained sections (white boxes) within the corresponding ROIs are shown. Areas shown in (D) and (F) are higher magnifications of the ROIs shown in (C) and (E), and areas shown in (I) and (K) are higher magnifications of the ROIs shown in (H) and (J) (white boxes). Data represent mean ± SEM. **p < 0.01; n = 6–8/group. Scale bars represent 500 μm (A, C, E, H, J) and 100 μm (D, F, I, K).

(L–S) CD4 staining in spinal cord sections revealed a significant increase in the number of CD4$^+$ T cells in both (L) BALB/c and (P) C57BL/6 mice treated with MSC/IL-13, compared with MSC- or NaCl-treated mice 4 weeks after SCI. Representative photomicrographs of spinal cord sections treated with (M and Q) NaCl, (N and R) MSC, or (O and S) MSC/IL-13 from BALB/c and C57BL/6 mice, respectively, are shown. White arrowheads in (M–O) and (Q–S) indicate CD4$^+$ T cells. Data represent mean ± SEM. ***p < 0.0001, **p < 0.01, *p < 0.05; n = 7–11/group. Scale bars represent 50 μm (M–O, Q–S).

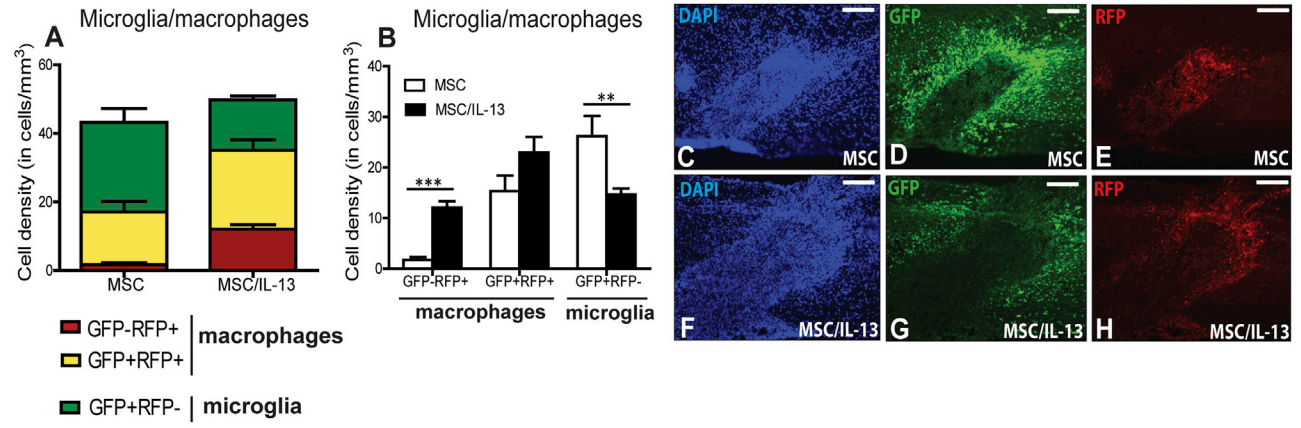

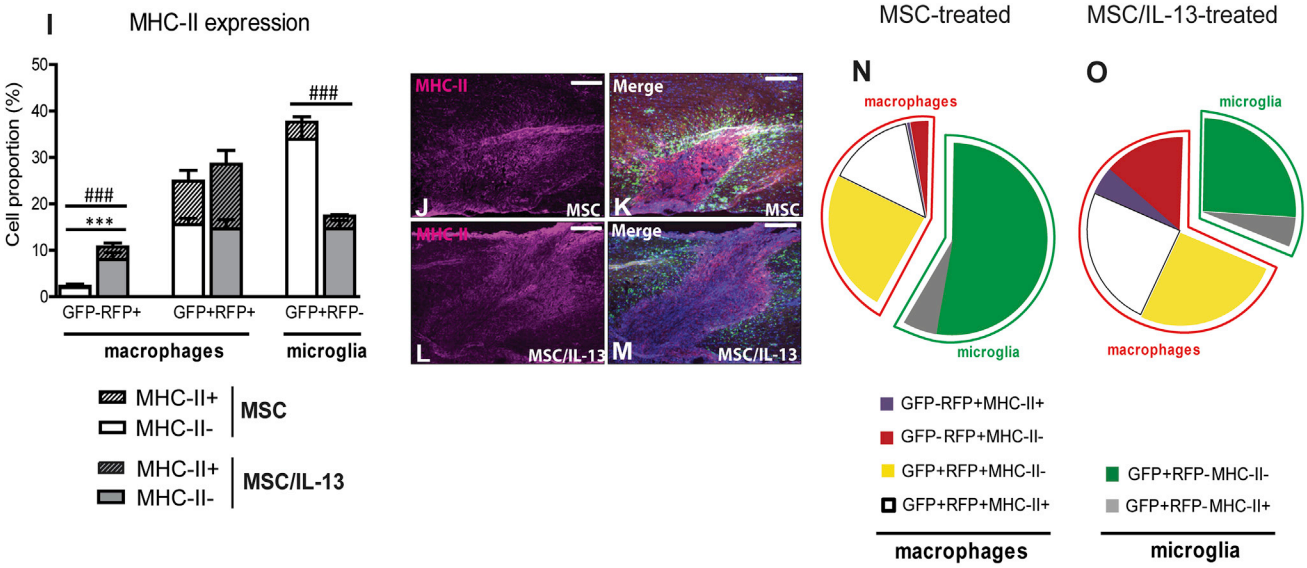

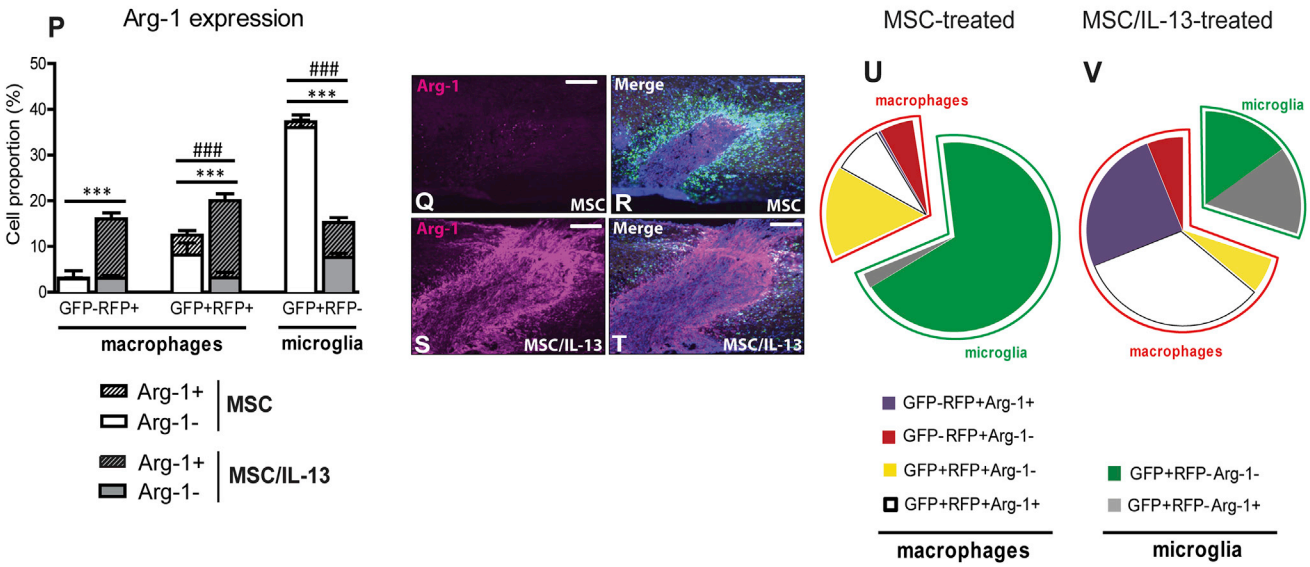

(legend on next page)

macrophages visible at the lesion site. These macrophages in turn appear to undergo alternative activation, thereby providing neuroprotection and improved therapeutic outcome following SCI.

Transplantation of MSC/IL-13 Decreases the Number of Macrophage-Axon Interactions

Finally, we investigated how the presence of alternatively activated microglia and macrophages at the lesion site following MSC/IL-13 grafting may have influenced the corresponding SCI pathology in both BALB/c (Figure 6A) and C57BL/6 (Figure 6H) mice. For this, we quantified the number of microglia/macrophage-axon interactions using IBA-1 and neurofilament staining. In both mouse backgrounds, we analyzed two areas rostral and caudal from the lesion epicenter (Figures 6B–6D and 6I–6K, white boxes) and counted the number of microglia/macrophage-axon contacts (Figures 6E–6G and 6L–6N). In BALB/c mice, we observed a significant decrease in the number of microglia/macrophage-axon contacts in both MSC-treated (Figure 6F) and MSC/IL-13-treated (Figure 6G) mice compared with NaCl control mice (Figure 6E). In C57BL/6 mice, we observed a significant decrease in the number of microglia/macrophage-axon contacts in MSC/IL-13-treated mice (Figure 6N) compared with MSC-treated (Figure 6M) and NaCl control mice (Figure 6L). These results indicate that both MSC and MSC/IL-13 (in a BALB/c background) and MSC/IL-13 (in a C57BL/6 background), may be driving activated macrophages located at the lesion site to a more alternatively activated, neuroprotective phenotype. This in turn leads to a reduction in the number of destructive macrophage-axon contacts.

DISCUSSION

The goal of this study was to compare the potentially beneficial properties and unravel key immune response changes following engraftment of control MSCs or MSCs overexpressing IL-13 in a well-established mouse SCI model. Although treatment with MSCs has been previously shown to exert positive effects in rodent models of SCI (Alexanian et al., 2011; Nakajima et al., 2012), their prolonged therapeutic effects and success in human clinical trials have been limited (Oh et al., 2016; Park et al., 2012). Genetic modification of MSCs, for example by overexpression of neurotrophic or growth factors, can further enhance their well-known beneficial effects and improve therapeutic outcome following CNS trauma (reviewed in Cui et al., 2013). In this study, we show that transplanted MSCs, which continuously secrete IL-13, significantly improve histopathological and functional recovery compared with NaCl controls following SCI in BALB/c and C57BL/6 mice. The correlation between histopathological (i.e., decreased lesion size, demyelinated area, and astrogliosis) and functional recovery was highly evident in C57BL/6 mice following grafting of IL-13-producing MSCs. Interestingly, in BALB/c mice, IL-13 contributed to histopathological recovery (decreased lesion size and demyelinated area), but did not further promote an additional functional

Figure 4. Transplantation of MSC/IL-13 Increases the Number of Neuroprotective, Alternatively Activated Macrophages and Decreases the Number of Microglia at the Graft Site

(A) Cell density quantification at the graft site revealed no significant differences in the total number of microglia/macrophages in MSC- or MSC/IL-13-treated mice.

(B) Further characterization of the microglia/macrophage populations revealed a significant increase in the number of $GFP^{-}RFP^{+}$ macrophages and a significant decrease in $GFP^{+}RFP^{-}$ microglia in MSC/IL-13-treated mice compared with MSC controls.

(C–H) $DAPI^{+}$ cells localize the position of the graft (C and F). Representative photomicrographs of (D and G) $CX_3CR1^{EGFP/+}$ microglia and (E and H) $CCR2^{RFP/+}$ macrophages are shown from MSC and MSC-IL-13-treated mice, respectively.

(I–O) Detailed phenotypic analysis of microglia/macrophage populations expressing MHC-II (I) revealed a significant increase in the number of $GFP^{-}RFP^{+}MHC\text{-}II^{+}$ and $GFP^{-}RFP^{+}MHC\text{-}II^{-}$ macrophages as well as a significant decrease in $GFP^{+}RFP^{-}MHC\text{-}II^{-}$ microglia in (L) MSC/IL-13-treated animals compared with (J) MSC controls. MHC-II activation is shown in the top shaded bar stacks, and $^{\#\#\#}$ represents significant differences in $MHC\text{-}II^{-}$ cells and *** in $MHC\text{-}II^{+}$ cells. A merged photomicrograph outlining the distribution of $DAPI^{+}/GFP^{+}/RFP^{+}/MHC\text{-}II^{+}$ cells at the graft site in (K) MSC- and (M) MSC/IL-treated animals is shown. The corresponding relative distribution of MHC-II-expressing microglia and macrophages at (N) control MSC and (O) MSC/IL-13 graft sites is shown.

(P–V) Analysis of microglia/macrophage populations expressing ARG-1 (P) revealed a significant increase in the number of $GFP^{-}RFP^{+}ARG\text{-}1^{+}$ and $GFP^{+}RFP^{+}ARG\text{-}1^{+}$ macrophages, $GFP^{+}RFP^{-}ARG\text{-}1^{+}$ microglia, as well as a significant decrease in the number of $GFP^{+}RFP^{+}ARG\text{-}1^{-}$ macrophages and $GFP^{+}RFP^{-}ARG\text{-}1^{-}$ microglia in (S) MSC/IL-13-treated animals compared with (Q) MSC controls. ARG-1 activation is shown in the top shaded bar stacks, and $^{\#\#\#}$ represents significant differences in $ARG\text{-}1^{-}$ cells and *** in $ARG\text{-}1^{+}$ cells. A merged photomicrograph outlining the distribution of $DAPI^{+}/GFP^{+}/RFP^{+}/ARG\text{-}1^{+}$ cells at the graft site in (R) MSC- and (T) MSC/IL-treated animals is shown. The corresponding relative distribution of ARG-1-expressing microglia and/or macrophages at (U) control MSC and (V) MSC/IL-13 graft sites is shown. Microglia and macrophages are encircled in red and green, respectively. Immunofluorescence colors: blue, DAPI; green, microglia; red, macrophages; magenta, $Arg1^{+}$ or $MHC\text{-}II^{+}$ microglia/macrophages.

Data represent mean ± SEM. ***$p < 0.0001$, $^{\#\#\#}p < 0.0001$, **$p < 0.01$; n = 6-11/group. All scale bars represent 200 μm.

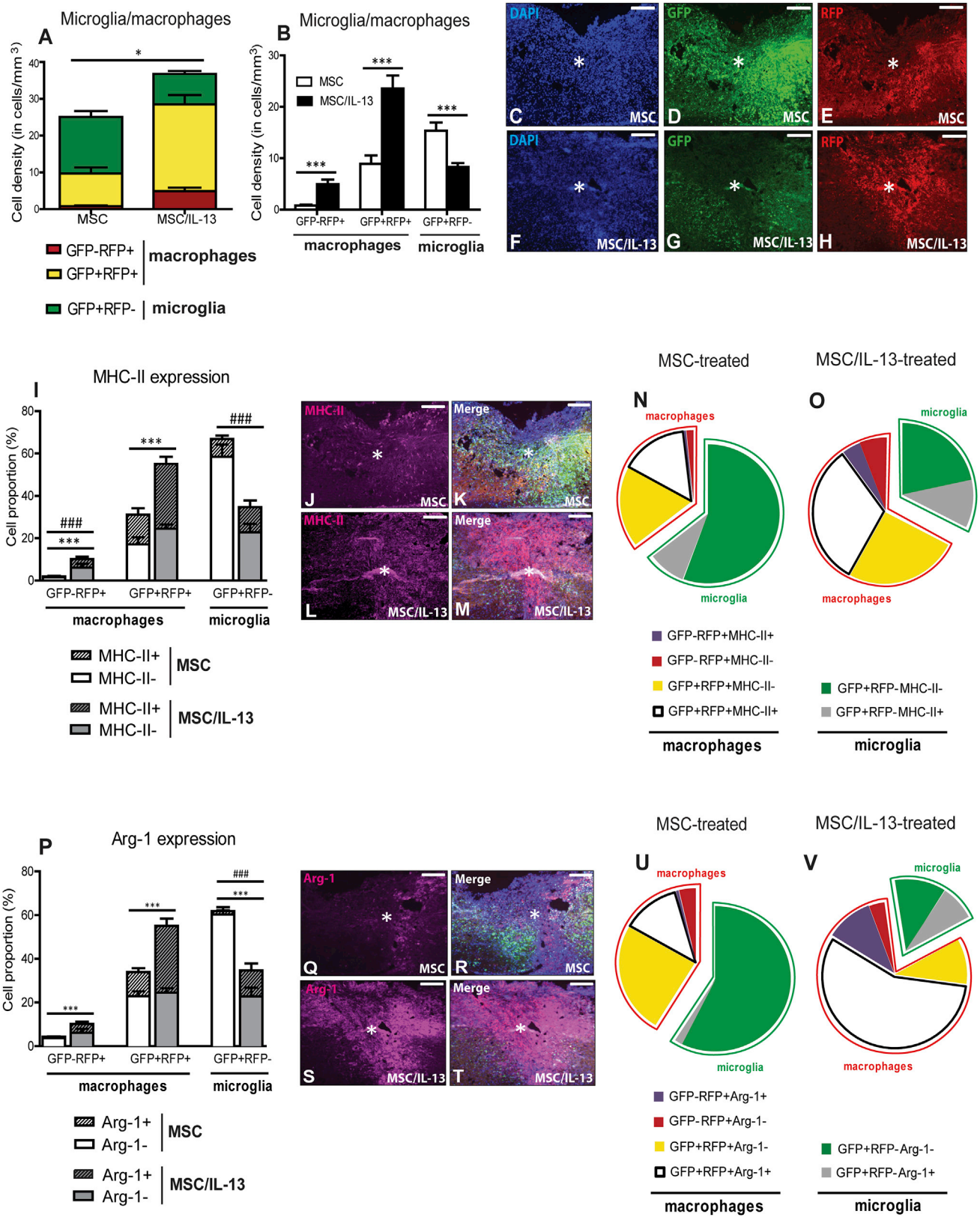

(legend on next page)

improvement induced by control MSCs. This variation may be attributed to the well-recognized immunological phenomenon that BALB/c mice are more T helper 2 (Th2) oriented while C57BL/6 are more Th1 oriented (Mills et al., 2000; Sellers et al., 2012). In addition, it has been reported that BALB/c mice display a higher recovery following SCI compared with C57BL/6 mice as measured using the BMS (Basso et al., 2006). This may explain the 1-point difference in the final BMS score between BALB/c and C57BL/6 mice (score of ~4 versus ~3, respectively). Furthermore, these data suggest that treatment with IL-13 may be unable to further enhance what is already a rather Th2-primed microenvironment (Hendrix and Nitsch, 2007) resulting in a ceiling effect in BALB/c mice.

It has been well described that IL-13 is capable of polarizing microglia and macrophages toward an alternatively activated M2a phenotype (Hoornaert et al., 2016; Van Dyken and Locksley, 2013). Therefore, we first investigated whether transplantation of MSCs secreting IL-13 could influence the microglia/macrophage phenotype in vivo within the MSC graft site. Our data confirm that MSC graft-associated microglia/macrophages can be efficiently driven toward an ARG-1-expressing state of alternative activation in vivo, in both BALB/c and C57BL/6 mice. Given the detrimental effect on microglia/macrophage cell number following treatment with MSC or MSC/IL-13, we consider cell phenotype (classically or alternatively activated) to be the most critical factor of interest when determining effects on functional outcome. Further discrimination between MSC-associated microglia and macrophages following grafting of IL-13-producing MSCs in $CX_3CR1^{EGFP/+}$ $CCR2^{RFP/+}$ C57BL/6 mice revealed that the majority of ARG-1-expressing cells are of peripheral monocyte/macrophage origin. The peripheral origin of ARG-1-expressing cells is, however, not surprising as control MSC grafts already attract, in addition to microglia, high numbers of peripheral monocytes/macrophages. Subsequently, IL-13 is able to further modulate the MSC graft site by increasing the number of ARG-1-expressing macrophages and microglia and decreasing the overall number of microglia. Although subject to debate and further investigation, we may argue that ARG-1-expressing microglia and macrophages are induced in situ upon contact with IL-13-secreting MSCs, rather than being specifically attracted.

T cell analysis within the spinal cord showed a significantly increased number of $CD4^+$ T cells in animals treated with MSC/IL-13. The specific subtype of the T cells is unclear, and previous studies from our group revealed that specific T cell immunophenotyping after CNS injury can be challenging and prone to artifacts, due to the low number of T cells present in the CNS (Hendrix et al., 2012). The high number of T cells in MSC/IL-13-treated mice may be due to the restriction of T cell chemotaxis by IL-13 (Tan et al., 1995), thereby leading to an accumulation of T cells within an area where they are highly activated. Since transplantation of MSC/IL-13 exerts beneficial effects on the injured spinal cord, it is tempting to speculate that

Figure 5. Transplantation of MSC/IL-13 Increases the Number of Infiltrating Neuroprotective, Alternatively Activated Macrophages and Decreases the Number of Microglia at the Lesion Site

(A) Cell-density quantification at the graft site revealed a significant increase in the number of microglia/macrophages present in MSC/IL-13-treated animals compared with MSC-treated animals.

(B) Further characterization of the microglia/macrophage populations revealed a significant increase in the number of GFP^-RFP^+ and GFP^+RFP^+ macrophages as well as a significant decrease in GFP^+RFP^- microglia in MSC/IL-13-treated mice compared with MSC controls.

(C–H) $DAPI^+$ cells localize the lesion site (C and F). Asterisk denotes the lesion epicenter. Representative photomicrographs of (D and G) $CX_3CR1^{EGFP/+}$ microglia and (E and H) $CCR2^{RFP/+}$ macrophages at the lesion site are shown from MSC- and MSC-IL-13-treated mice, respectively.

(I–O) Detailed phenotypic analysis of microglia/macrophage populations expressing MHC-II (I) revealed a significant increase in the number of $GFP^-RFP^+MHC\text{-}II^+$ and $GFP^-RFP^+MHC\text{-}II^-$ macrophages as well as a significant decrease in $GFP^+RFP^-MHC\text{-}II^-$ microglia in (L) MSC/IL-13-treated animals compared with (J) MSC controls. MHC-II activation is shown in the top shaded bar stacks, and $^{###}$ represents significant differences in $MHC\text{-}II^-$ cells and *** in $MHC\text{-}II^+$ cells. A merged photomicrograph outlining the distribution of $DAPI^+/GFP^+/RFP^+/MHC\text{-}II^+$ cells at the lesion site in (K) MSC and (M) MSC/IL-treated animals is shown. The corresponding relative distribution of MHC-II-expressing microglia and macrophages at (N) control MSC and (O) MSC/IL-13 lesion sites is shown.

(P–V) Analysis of microglia/macrophage populations expressing ARG-1 (P) revealed a significant increase in the number of $GFP^-RFP^+ARG\text{-}1^+$, $GFP^+RFP^+ARG\text{-}1^+$ macrophages, and $GFP^+RFP^-ARG\text{-}1^+$ microglia, as well as a significant decrease in the number of $GFP^+RFP^+ARG\text{-}1^-$ macrophages and $GFP^+RFP^-ARG\text{-}1^-$ microglia in (S) MSC/IL-13-treated animals compared with (Q) MSC controls. ARG-1 activation is shown in the top shaded bar stacks, and $^{###}$ represents significant differences in $ARG\text{-}1^-$ cells and *** in $ARG\text{-}1^+$ cells. A merged photomicrograph outlining the distribution of $DAPI^+/GFP^+/RFP^+/ARG\text{-}1^+$ cells at the lesion site in (R) MSC- and (T) MSC/IL-treated animals is shown. The corresponding relative distribution of ARG-1-expressing microglia and macrophages at (U) control MSC and (V) MSC/IL-13 graft sites is shown. Microglia and macrophages are encircled in red and green, respectively. Immunofluorescence colors: blue, DAPI; green, microglia; red, macrophages; magenta, $Arg1^+$ or $MHC\text{-}II^+$ microglia/macrophages.

Data represent mean ± SEM. ***$p < 0.0001$, $^{###}p < 0.0001$, *$p < 0.05$; n = 9–14/group. All scale bars represent 200 μm.

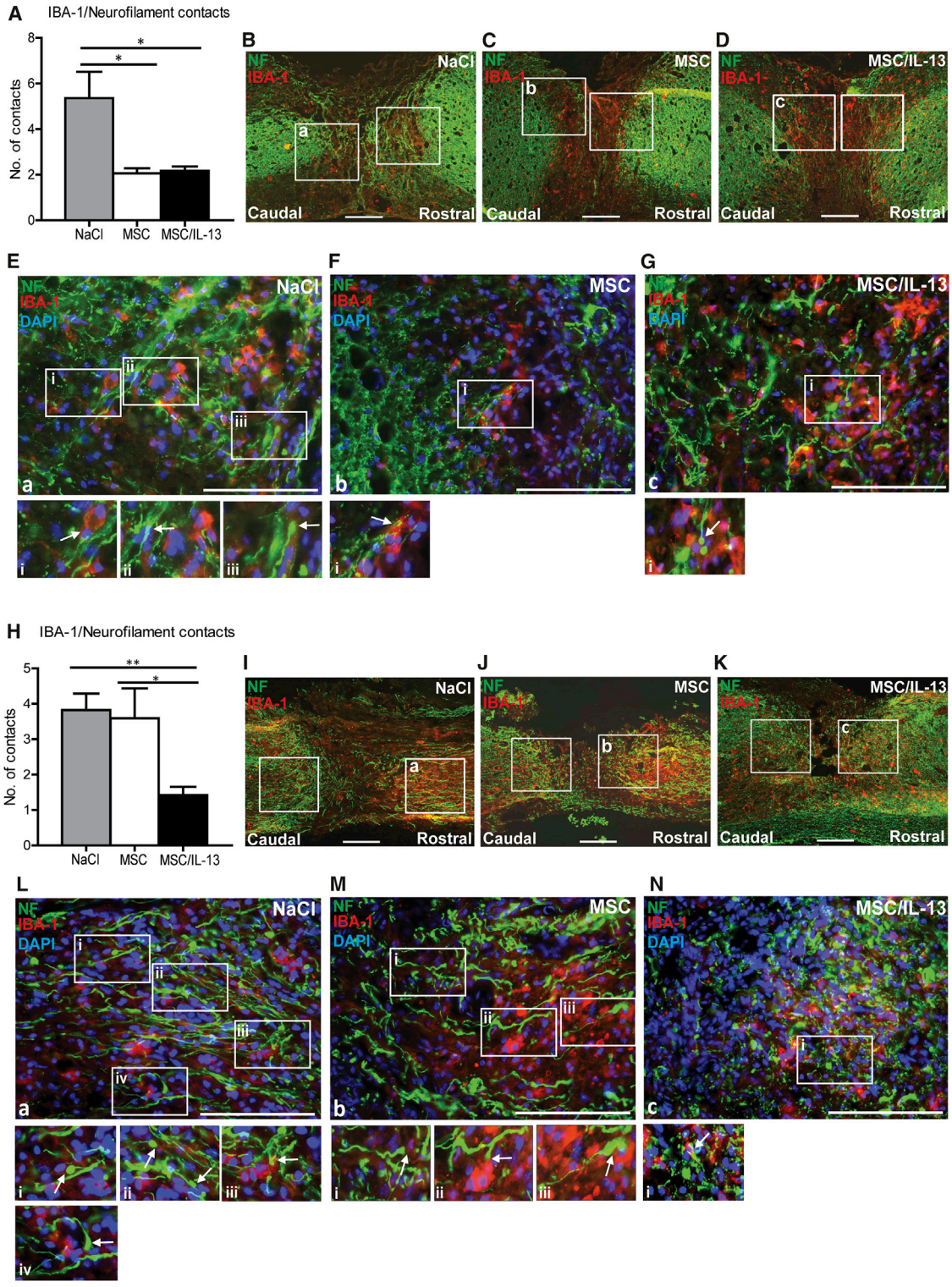

Figure 6. Transplantation of MSC/IL-13 Decreases the Number of Microglia/Macrophage-Axon Contacts

(A–G) Quantification of microglia/macrophage and axon contacts in BALB/c mice following staining for IBA-1 and neurofilament, respectively (A), revealed a significant decrease in the number of contacts in both MSC- and MSC/IL-13-treated mice compared with NaCl controls. Representative photomicrographs from (B) NaCl-treated, (C) MSC-treated, and (D) MSC/IL-13-treated BALB/c mice indicate the

(legend continued on next page)

the attracted T cells are also those with beneficial properties (Hendrix and Nitsch, 2007).

As the introduction of alternatively activated microglia and macrophages is established by the presence of IL-13 at the graft site, we hypothesized that a phenotypic shift in the microglia/macrophage response may also be possible at the site of the spinal cord lesion. Similarly to our observations at the MSC/IL-13 graft site, we observed an increase in ARG-1-expressing macrophages and microglia and an overall decrease in microglia at the lesion site in mice receiving MSC/IL-13 grafts. An interesting question consequently arises as to how ARG-1-expressing microglia/macrophages are induced at the lesion site. We can speculate that the induction of alternatively activated microglia/macrophages at the lesion site may be due to passive diffusion of IL-13 from the MSC/IL-13 graft site. Upon contact with lesion-associated microglia or infiltrating macrophages, this may in turn result in a shift toward a more neuroprotective cell phenotype. Although this hypothesis seems highly plausible, one cannot exclude the possibility that other factors (aside from IL-13), may be secreted from the MSC graft or alternatively activated microglia/macrophages at the MSC/IL-13 graft site. These derived factors, either alone or in combination, may also influence the phenotypic properties of lesion-associated microglia/macrophages. Furthermore, as discussed above, specific recruitment of alternatively activated monocytes/macrophages directly from peripheral blood may not be evident, although their recruitment via the MSC/IL-13 graft site cannot be excluded. An important observation to be taken into consideration for future experiments is the presence of the double-positive $CX_3CR1^{EGFP/+}$ $CCR2^{RFP/+}$ cell population. We, as well as others, hypothesize that these double-positive cells are blood-derived macrophages given the known limitation that $CCR2^{RFP/+}$ monocytes can downregulate their reporter over time and show phenotypic evolution (Yamasaki et al., 2014). It has also been shown that resident microglia consist primarily of $CX_3CR1^{EGFP/+}$ cells, while blood-derived macrophages are made up of both $CX_3CR1^{EGFP/+}$ and $CCR2^{RFP/+}$ macrophage populations (Evans et al., 2014). In this study, we therefore consider these double-positive cells to be part of the macrophage population. The arrival of promising microglia-specific markers (Bennett et al., 2016; Greenhalgh et al., 2016) may be useful in future studies to clarify whether the double-positive cells are primarily infiltrating macrophages. It is clear that evaluation of the inflammatory infiltrate is complex, and variation occurs not only in the type of disease/trauma model but also in the time point under investigation.

Although the variation in immunological background between BALB/c and C57BL/6 is a well-known phenomenon (Mills et al., 2000; Sellers et al., 2012), we have not observed any immunological differences in our transplantation systems in either mouse strain. As shown in this study, transplantation of MSC/IL-13 leads to a significant increase in $Arg1^+$ cells at the graft sites in both BALB/c and C57BL/6 mice (Figures 3G and 4P, respectively). Additionally our group has performed an in-depth analysis of graft-site remodeling upon MSC transplantation in the CNS of BALB/c, FBV, or C57BL/6 mouse backgrounds (De Vocht et al., 2013; Hoornaert et al., 2016; Le Blon et al., 2014). Upon MSC transplantation in all of the above mouse strains, cells undergo hypoxic stress within the first 24 hr and the core of the graft becomes apoptotic and necrotic. This is followed by early infiltration of neutrophils on day 1. From days 3 to 7, the graft becomes infiltrated by macrophages and surrounded by microglia. At this point astrocytes begin forming a barrier, which encapsulates the graft (Le Blon et al., 2016). Based on these studies and our current results, we conclude that there is no obvious difference in the graft-site response between BALB/c and C57BL/6 mice.

Finally, we suggest a potential mode of action for the observed neuroprotective effects following grafting of IL-13-producing MSCs. Based on our data, and in agreement with current literature, we can put forward two mechanistic explanations. Firstly, it has been shown that a reduction in CX_3CR1 signaling on microglia/macrophages reduces their proinflammatory nature and leads to improved outcome following SCI (Donnelly et al., 2011). Therefore, the decrease in $EGFP^+RFP^-$ microglia, which we observed at the lesion site following grafting of MSC/IL-13, may correlate with the improved functional outcome shown in MSC/IL-13-treated mice following

areas (two white boxed regions) where microglia/macrophage and axon contacts were quantified rostral and caudal from the lesion epicenter. A larger magnification of the white boxes labeled (a), (b), and (c) are shown in (E), (F), and (G), respectively. The white boxed regions (i–iii) in photomicrographs (E–G) are shown at a higher magnification to indicate examples of microglia/macrophage and axon contacts (white arrows).

(H–N) Quantification of microglia/macrophage and axon contacts in C57BL/6 mice revealed a significant decrease in the number of contacts in MSC/IL-13-treated C57BL/6 mice compared with MSC and NaCl controls (H). Representative photomicrographs of the areas quantified (two white boxed regions) are shown from (I) NaCl-treated, (J) MSC-treated, and (K) MSC/IL-13-treated mice. A larger magnification of the white boxes labeled (a), (b), and (c) are shown in (L), (M), and (N), respectively. The white boxed regions (i–iv) in photomicrographs (L–M) are shown at a higher magnification to indicate examples of microglia/macrophage and axon contacts (white arrows). Scale bars represent 200 μm (B–D, I–K) and 50 μm (E–G, L–N). Data represent mean ± SEM. $^{**}p < 0.01$, $^{*}p < 0.05$; n = 4–10/group.

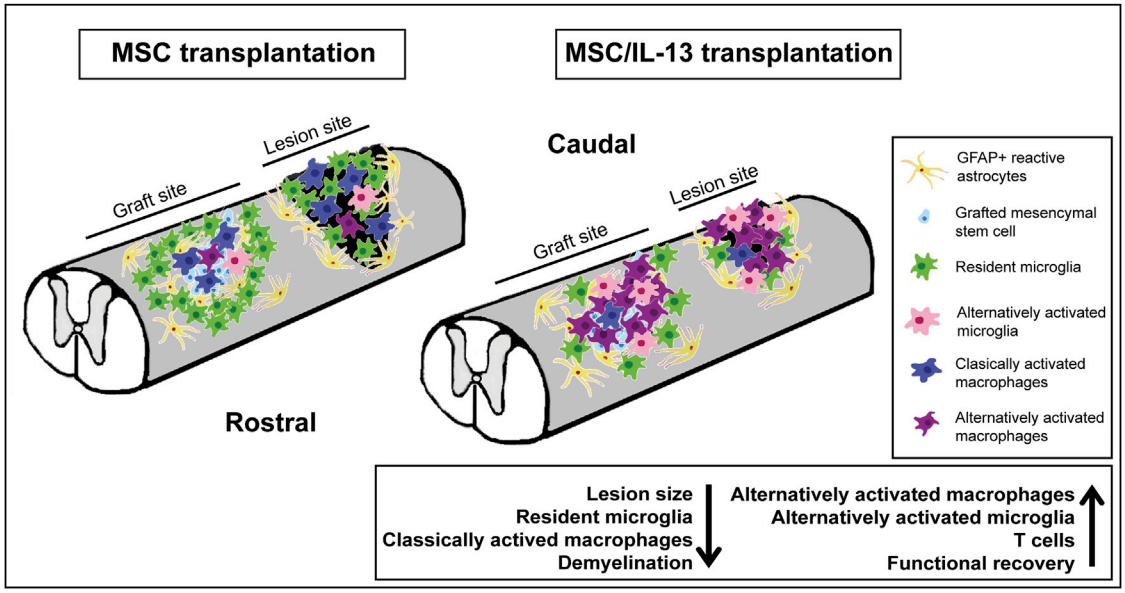

Figure 7. Schematic Representation of the Lesion and Graft Site in MSC Compared with MSC/IL-13-Treated Mice Following SCI

In MSC-treated mice, the lesion and graft site contain classically activated macrophages as well as a low number of alternatively activated macrophages and microglia. Both regions are encapsulated by GFAP$^+$ astrocytes. The lesion area consists of resident microglia within and around the lesion site, while the graft site contains resident microglia at the graft border. Following treatment with MSC/IL-13, the histological appearance and cell distribution differs substantially within the spinal cord. There is a decrease in lesion size as well as classically activated macrophages and resident microglia at both the lesion and graft site. There is also a dramatic increase in the number of alternatively activated macrophages and microglia at both the lesion and graft site. Both the lesion and graft sites remain encapsulated by GFAP$^+$ astrocytes. Treatment with MSC/IL-13 alters the immune cell distribution and phenotype, leading to improved functional recovery in a mouse model of SCI.

SCI. The way in which IL-13 actually reduces the number of microglia in this model remains speculative; however, it may be explained by a previously described ability of IL-13 to directly induce apoptosis in activated microglia (Yang et al., 2006). Secondly, it has recently been demonstrated that CNS axons undergo lengthy retraction from the site of damage following SCI and that activated macrophages play a direct role in this retraction via destructive physical interactions with the injured axons (Busch et al., 2009; Evans et al., 2014; Horn et al., 2008). Therefore, the observed conversion of lesion-infiltrating macrophages into an ARG-1-expressing alternatively activated phenotype upon MSC/IL-13 grafting may have rendered these cells less neurodestructive. The latter suggests a correlation with the significant decrease in macrophage-axon contacts observed at the lesion site in BALB/c mice following treatment with MSC or MSC/IL-13 and in C57BL/6 mice following treatment with MSC/IL-13. It is tempting to speculate that a corresponding reduction in axonal dieback may lead to the significantly improved histopathological and functional outcome observed following SCI. We hypothesize that an increase in alternatively activated macrophages and microglia may promote wound healing, regeneration, and functional recovery via the secretion of proregenerative factors such as IL-10, insulin-like growth factor-1, and vascular endothelial growth factor A (Röszer, 2015). Taken together, these data provide evidence that MSCs can be successfully used as carriers for the local delivery of a beneficial cytokine such as IL-13 and lead to improved functional and histopathological recovery in a mouse model of SCI (Figure 7).

EXPERIMENTAL PROCEDURES

Animals

Wild-type (WT) BALB/c OlaHsd (strain code 162) and WT C57BL/6 mice (strain code 027) were obtained from Harlan and Charles River Laboratories, respectively. $CX_3CR1^{EGFP/EGFP}$ mice (strain code 005582) and $CCR2^{RFP/RFP}$ mice (strain code 017586) were obtained from Jackson Laboratories. $CX_3CR1^{EGFP/+}$ $CCR2^{RFP/+}$ mice were obtained by breeding $CX_3CR1^{EGFP/EGFP}$ mice with $CCR2^{RFP/RFP}$ mice. Resulting double transgenic mice have one allele of the CX_3CR1 gene replaced by EGFP and the other allele of the CCR2 gene replaced by RFP (Mizutani et al., 2012). This results in the presence of green fluorescent microglia ($EGFP^+RFP^-$) and red fluorescent infiltrating macrophages/monocytes ($EGFP^-RFP^+$ and $EGFP^+RFP^+$). See Supplemental Experimental Procedures for further details. Male mice were used for all experiments, except for those carried out in $CX_3CR1^{EGFP/+}$ $CCR2^{RFP/+}$ mice, where equal numbers of males and females were used. All experiments were performed using 8- to 10-week-old mice, and were approved by the

local ethical committees and performed according to the guidelines described on the protection of animals used for scientific purposes at Hasselt University (EU Directives 2010/63) and University of Antwerp (2011/13 and 2012/39).

Isolation, Genetic Engineering, and Culturing of MSCs

In this study we used two previously established and characterized bone marrow-derived MSC lines originally derived from BALB/c and C57BL/6 mice (Hoornaert et al., 2016; Le Blon et al., 2014). Both the parental BALB/c and C57BL/6 MSC lines, as well as derivatives thereof genetically engineered to express IL-13, were used for transplantation experiments. See Supplemental Experimental Procedures for further details.

Spinal Cord Hemisection Injury

A T-cut spinal cord hemisection injury was performed as previously described (Boato et al., 2010; Dooley et al., 2016; Geurts et al., 2015; Nelissen et al., 2013; Vangansewinkel et al., 2016; Vidal et al., 2013). See Supplemental Experimental Procedures for further details.

Cell Transplantation

For transplantation experiments, MSC and MSC/IL-13 cell populations were harvested via trypsin-EDTA treatment. Cells were then washed twice with NaCl, resuspended in NaCl, and kept on ice until spinal cord transplantation. The animals were divided into three groups: those receiving an injection of MSCs, MSC/IL-13, or NaCl (control). See Supplemental Experimental Procedures for further details. For transplantation experiments carried out in $CX_3CR1^{EGFP/+}$ $CCR2^{RFP/+}$ mice, no NaCl control group used, given that the research objectives in question concerned potential differences between IL-13-secreting MSCs and control MSCs. Furthermore, 1.5×10^5 cells were grafted to allow for more detailed histological quantification.

Locomotion Tests

Starting 1 day after surgery, functional recovery in SCI mice was measured for 4 weeks using the BMS (Basso et al., 2006). See Supplemental Experimental Procedures for further details.

Immunofluorescence Analysis

Spinal cord cryosections (10 μm) were obtained from animals transcardially perfused 4 weeks post injury with Ringer solution containing heparin, followed by 4% paraformaldehyde in 0.1 M PBS, and immunofluorescence analysis was performed as previously described (Boato et al., 2010; Dooley et al., 2016; Geurts et al., 2015; Nelissen et al., 2013; Vangansewinkel et al., 2016). See Supplemental Experimental Procedures for further details.

Histological Quantification in WT BALB/c and WT C57BL/6 Mice

For measurement of lesion size and demyelinated area, five to seven sections per animal (WT BALB/c: n = 6–8 animals per group; WT C57BL/6: n = 9–10 animals per group) containing the lesion center as well as consecutive rostral and caudal areas were analyzed, as previously described (Boato et al., 2010; Dooley et al., 2016; Geurts et al., 2015; Nelissen et al., 2013; Vangansewinkel et al., 2016). To quantify classically activated and alternatively activated microglia/macrophages at the lesion or graft site, we stained sections for MHC-II and ARG-1, respectively. Quantification of microglia/macrophage and axon interactions was performed by counting the number of contacts between neurofilament$^+$ dystrophic axon bulbs and IBA-1$^+$ microglia/macrophages. See Supplemental Experimental Procedures for further details.

Histological Quantification in $CX_3CR1^{EGFP/+}$ $CCR2^{RFP/+}$ Mice

For quantitative phenotypic analyses of macrophage and/or microglia responses at both the lesion and graft site, five to seven sections per animal (graft: n = 6–11 animals per group; lesion: n = 9–14 animals per group) were analyzed using TissueQuest immunofluorescence analysis software 14 days post injury (TissueGnostics v3.0), as previously described (De Vocht et al., 2013; Hoornaert et al., 2016; Le Blon et al., 2014). For each of region of interest (graft/lesion site), an entire picture taken at 10× magnification was used for quantification and the surface area in the xy plane was determined. According to previously established procedures, the following parameters were quantified at the lesion and graft site: the cellular density of EGFP$^-$RFP$^+$ macrophages ($CCR2^{RFP/+}$), EGFP$^+$RFP$^+$ double-positive microglia/macrophages ($CX_3CR1^{EGFP/+}$ $CCR2^{RFP/+}$), as well as EGFP$^+$RFP$^-$ microglia ($CX_3CR1^{EGFP/+}$) in both MSC and MSC/IL-13-treated groups. Although the presence of a double-positive $CX_3CR1^{EGFP/+}$ $CCR2^{RFP/+}$ population is prominent, we hypothesize that these cells are blood derived and of peripheral origin, given that it is a known limitation that $CCR2^{RFP/+}$ monocytes can downregulate their reporter over time and show phenotypic evolution (Yamasaki et al., 2014). Based on the above cell-density calculations, the proportion of microglia or macrophages at the graft and lesion site expressing MHC-II or ARG-1 were calculated as follows: (1) EGFP$^-$RFP$^+$MHC-II$^+$/ARG-1$^+$ cells, (2) EGFP$^+$RFP$^+$MHC-II$^+$/ARG-1$^+$ cells, (3) EGFP$^+$RFP$^-$MHC-II$^+$/ARG-1$^+$ cells, (4) EGFP$^-$RFP$^+$MHC-II$^-$/ARG-1$^-$ cells, (5) EGFP$^+$RFP$^+$MHC-II$^-$/ARG-1$^-$ cells, (6) EGFP$^+$RFP$^-$MHC-II$^-$/ARG-1$^-$ cells. Put simply, we identify the number of classically or alternatively activated $CCR2^{RFP/+}$ macrophages and $CX_3CR1^{EGFP/+}$ $CCR2^{RFP/+}$ macrophages or $CX_3CR1^{EGFP/+}$ microglia, at both the graft and lesion site.

Statistical Analysis

All statistical analyses were performed using Prism 5.0 software (GraphPad). The BMS locomotion tests as well as histological evaluation of astrogliosis and microglia/macrophage intensities were analyzed using two-way ANOVA for repeated measurements with Bonferroni correction for multiple comparisons. All other differences between two groups were evaluated using the nonparametric Mann-Whitney U test. Differences were considered statistically significant when $p < 0.05$. Data shown represent mean values per experimental group ±SEM.

SUPPLEMENTAL INFORMATION

Supplemental Information includes Supplemental Experimental Procedures and can be found with this article online at http://dx.doi.org/10.1016/j.stemcr.2016.11.005.

AUTHOR CONTRIBUTIONS

D.D. participated in the study design, surgical procedures, collection and/or assembly of data, data analysis/interpretation, and manuscript writing. E.L. participated in the study design, data analysis/interpretation, and manuscript writing. T.V., D.l.B., and C.H. participated in the study design and data analysis/interpretation. P.P. and S.H. participated in the study conception and coordination, and helped to draft the final manuscript. All authors read and approved the final manuscript.

ACKNOWLEDGMENTS

The authors would like to acknowledge Dr. Leen Timmermans for her excellent technical assistance. This manuscript was supported in part by grants from Fonds Wetenschappelijk Onderzoek – Vlaanderen awarded to S.H. (G.0834.11N, G.0389.12), E.L. (G6058.13N), and P.P. (G.0130.11, G.0131.11, G.0834.11N). D.D. is a PhD student at the Transnational University Limburg and the University of Antwerp. C.H. holds a PhD studentship from the FWO Vlaanderen. At the time of this study, T.V. and D.l.B. held PhD studentships from the Flemish Institute for Science and Technology (IWT Vlaanderen).

Received: July 14, 2016
Revised: November 10, 2016
Accepted: November 10, 2016
Published: December 13, 2016

REFERENCES

Alexanian, A.R., Fehlings, M.G., Zhang, Z., and Maiman, D.J. (2011). Transplanted neurally modified bone marrow-derived mesenchymal stem cells promote tissue protection and locomotor recovery in spinal cord injured rats. Neurorehabil. Neural Repair *25*, 873–880.

Basso, D.M., Fisher, L.C., Anderson, A.J., Jakeman, L.B., McTigue, D.M., and Popovich, P.G. (2006). Basso Mouse Scale for locomotion detects differences in recovery after spinal cord injury in five common mouse strains. J. Neurotrauma *23*, 635–659.

Bennett, M.L., Bennett, F.C., Liddelow, S.A., Ajami, B., Zamanian, J.L., Fernhoff, N.B., Mulinyawe, S.B., Bohlen, C.J., Adil, A., Tucker, A., et al. (2016). New tools for studying microglia in the mouse and human CNS. Proc. Natl. Acad. Sci. USA *113*, E1738–E1746.

Boato, F., Hendrix, S., Huelsenbeck, S.C., Hofmann, F., Große, G., Djalali, S., Klimaschewski, L., Auer, M., Just, I., Ahnert-Hilger, G., et al. (2010). C3 peptide enhances recovery from spinal cord injury by improved regenerative growth of descending fiber tracts. J. Cell Sci. *123*, 1652–1662.

Bogie, J.J., Stinissen, P., and Hendriks, J.A. (2014). Macrophage subsets and microglia in multiple sclerosis. Acta Neuropathol. *128*, 191–213.

Boyle, W.J., Simonet, W.S., and Lacey, D.L. (2003). Osteoclast differentiation and activation. Nature *423*, 337–342.

Bruce-Keller, A.J., Barger, S.W., Moss, N.I., Pham, J.T., Keller, J.N., and Nath, A. (2001). Pro-inflammatory and pro-oxidant properties of the HIV protein Tat in a microglial cell line: attenuation by 17β-estradiol. J. Neurochem. *78*, 1315–1324.

Busch, S.A., Horn, K.P., Silver, D.J., and Silver, J. (2009). Overcoming macrophage-mediated axonal dieback following CNS injury. J. Neurosci. *29*, 9967–9976.

Cash, E., Minty, A., Ferrara, P., Caput, D., Fradelizi, D., and Rott, O. (1994). Macrophage-inactivating IL-13 suppresses experimental autoimmune encephalomyelitis in rats. J. Immunol. *153*, 4258–4267.

Colton, C. (2009). Heterogeneity of microglial activation in the innate immune response in the brain. J. Neuroimmune Pharmacol. *4*, 399–418.

Cui, X., Chen, L., Ren, Y., Ji, Y., Liu, W., Liu, J., Yan, Q., Cheng, L., and Sun, Y. (2013). Genetic modification of mesenchymal stem cells in spinal cord injury repair strategies. Bioscience Trends *7*, 202–208.

De Vocht, N., Praet, J., Reekmans, K., Le Blon, D., Hoornaert, C., Daans, J., Berneman, Z., Van der Linden, A., and Ponsaerts, P. (2013). Tackling the physiological barriers for successful mesenchymal stem cell transplantation into the central nervous system. Stem Cell Res. Ther. *4*, 101.

Doherty, T.M., Kastelein, R., Menon, S., Andrade, S., and Coffman, R.L. (1993). Modulation of murine macrophage function by IL-13. J. Immunol. *151*, 7151–7160.

Donnelly, D.J., Longbrake, E.E., Shawler, T.M., Kigerl, K.A., Lai, W., Tovar, C.A., Ransohoff, R.M., and Popovich, P.G. (2011). Deficient CX3CR1 signaling promotes recovery after mouse spinal cord injury by limiting the recruitment and activation of ly6C(lo)/iNOS(+) macrophages. J. Neurosci. *31*, 9910–9922.

Dooley, D., Vidal, P., and Hendrix, S. (2013). Immunopharmacological intervention for successful neural stem cell therapy: new perspectives in CNS neurogenesis and repair. Pharmacol. Ther. *141*, 21–31.

Dooley, D., Lemmens, E., Ponsaerts, P., and Hendrix, S. (2016). Interleukin-25 is detrimental for recovery after spinal cord injury in mice. J. Neuroinflammation *13*, 1–6.

Doyle, A.G., Herbein, G., Montaner, L.J., Minty, A.J., Caput, D., Ferrara, P., and Gordon, S. (1994). Interleukin-13 alters the activation state of murine macrophages in vitro: comparison with interleukin-4 and interferon-γ. Eur. J. Immunol. *24*, 1441–1445.

Evans, T.A., Barkauskas, D.S., Myers, J., Hare, E.G., You, J., Ransohoff, R.M., Huang, A.Y., and Silver, J. (2014). High-resolution intravital imaging reveals that blood derived macrophages but not resident microglia facilitate secondary axonal dieback in traumatic spinal cord injury. Exp. Neurol. *254*, 109–120.

Geurts, N., Vangansewinkel, T., Lemmens, S., Nelissen, S., Geboes, L., Schwartz, C., Voehringer, D., and Hendrix, S. (2015). Basophils are dispensable for the recovery of gross locomotion after spinal cord hemisection injury. J. Leukoc. Biol. *99*, 579–582.

Gordon, S. (2003). Alternative activation of macrophages. Nat. Rev. Immunol. *3*, 23–35.

Greenhalgh, A.D., Passos dos Santos, R., Zarruk, J.G., Salmon, C.K., Kroner, A., and David, S. (2016). Arginase-1 is expressed exclusively by infiltrating myeloid cells in CNS injury and disease. Brain Behav. Immun. *56*, 61–67.

Hendrix, S., and Nitsch, R. (2007). The role of T helper cells in neuroprotection and regeneration. J. Neuroimmunology *184*, 100–112.

Hendrix, S., Kramer, P., Pehl, D., Warnke, K., Boato, F., Nelissen, S., Lemmens, E., Pejler, G., Metz, M., Siebenhaar, F., et al. (2012). Mast cells protect from post-traumatic brain inflammation by the mast cell-specific chymase mouse mast cell protease-4. FASEB J. *3*, 920–929.

Hoornaert, C.J., Luyckx, E., Reekmans, K., Dhainaut, M., Guglielmetti, C., Le Blon, D., Dooley, D., Fransen, E., Daans, J., Verbeeck, L., et al. (2016). In vivo interleukin-13-primed macrophages contribute to reduced alloantigen-specific T cell activation and prolong immunological survival of allogeneic mesenchymal stem cell implants. Stem Cells *34*, 1971–1984.

Horn, K.P., Busch, S.A., Hawthorne, A.L., van Rooijen, N., and Silver, J. (2008). Another barrier to regeneration in the CNS: activated macrophages induce extensive retraction of dystrophic axons through direct physical interactions. J. Neurosci. *28*, 9330–9341.

Le Blon, D., Hoornaert, C., Daans, J., Santermans, E., Hens, N., Goossens, H., Berneman, Z., and Ponsaerts, P. (2014). Distinct spatial distribution of microglia and macrophages following mesenchymal stem cell implantation in mouse brain. Immunol. Cell Biol. *92*, 650–658.

Le Blon, D., Hoornaert, C., Detrez, J.R., Bevers, S., Daans, J., Goossens, H., De Vos, W.H., Berneman, Z., and Ponsaerts, P. (2016). Immune remodelling of stromal cell grafts in the central nervous system: therapeutic inflammation or (harmless) side-effect? J Tissue Eng. Regen. Med. http://dx.doi.org/10.1002/term.2188.

Mantovani, A., Sica, A., Sozzani, S., Allavena, P., Vecchi, A., and Locati, M. (2004). The chemokine system in diverse forms of macrophage activation and polarization. Trends Immunol. *25*, 677–686.

Martino, G., and Pluchino, S. (2006). The therapeutic potential of neural stem cells. Nat. Rev. Neurosci. *7*, 395–406.

Mills, C.D., Kincaid, K., Alt, J.M., Heilman, M.J., and Hill, A.M. (2000). M-1/M-2 macrophages and the Th1/Th2 paradigm. J. Immunol. *164*, 6166–6173.

Mizutani, M., Pino, P.A., Saederup, N., Charo, I.F., Ransohoff, R.M., and Cardona, A.E. (2012). The fractalkine receptor but not CCR2 is present on microglia from embryonic development throughout adulthood. J. Immunol. *188*, 29–36.

Nakajima, H., Uchida, K., Guerrero, A.R., Watanabe, S., Sugita, D., Takeura, N., Yoshida, A., Long, G., Wright, K.T., Johnson, W.E.B., et al. (2012). Transplantation of mesenchymal stem cells promotes an alternative pathway of macrophage activation and functional recovery after spinal cord injury. J. Neurotrauma *29*, 1614–1625.

Nelissen, S., Vangansewinkel, T., Geurts, N., Geboes, L., Lemmens, E., Vidal, P., Lemmens, S., Willems, L., Boato, F., Dooley, D., et al. (2013). Mast cells protect from post-traumatic spinal cord damage in mice by degrading inflammation-associated cytokines via mouse mast cell protease 4. Neurobiol. Dis. *62*, 260–272.

Ochoa-Repáraz, J., Rynda, A., Ascón, M.A., Yang, X., Kochetkova, I., Riccardi, C., Callis, G., Trunkle, T., and Pascual, D.W. (2008). IL-13 production by regulatory T cells protects against experimental autoimmune encephalomyelitis independently of autoantigen. J. Immunol. *181*, 954–968.

Offner, H., Subramanian, S., Wang, C., Afentoulis, M., Vandenbark, A.A., Huan, J., and Burrows, G.G. (2005). Treatment of passive experimental autoimmune encephalomyelitis in SJL mice with a recombinant TCR ligand induces IL-13 and prevents axonal injury. J. Immunol. *175*, 4103–4111.

Oh, S.K., Choi, K.H., Yoo, J.Y., Kim, D.Y., Kim, S.J., and Jeon, S.R. (2016). A phase iii clinical trial showing limited efficacy of autologous mesenchymal stem cell therapy for spinal cord injury. Neurosurgery *78*, 436–447.

Orlacchio, A., Bernardi, G., and Martino, S. (2010). Stem cells: an overview of the current status of therapies for central and peripheral nervous system diseases. Curr. Med. Chem. *17*, 595–608.

Park, J.H., Kim, D.Y., Sung, I.Y., Choi, G.H., Jeon, M.H., Kim, K.K., and Jeon, S.R. (2012). Long-term results of spinal cord injury therapy using mesenchymal stem cells derived from bone marrow in humans. Neurosurgery *70*, 1238–1247.

Protzer, U., Maini, M.K., and Knolle, P.A. (2012). Living in the liver: hepatic infections. Nat. Rev. Immunol. *12*, 201–213.

Rolls, A., Shechter, R., and Schwartz, M. (2009). The bright side of the glial scar in CNS repair. Nat. Rev. Neurosci. *10*, 235–241.

Röszer, T. (2015). Understanding the mysterious M2 macrophage through activation markers and effector mechanisms. Mediators Inflamm. *2015*, 16.

Sellers, R.S., Clifford, C.B., Treuting, P.M., and Brayton, C. (2012). Immunological variation between inbred laboratory mouse strains: points to consider in phenotyping genetically immunomodified mice. Vet. Pathol. *49*, 32–43.

Tan, J., Deleuran, B., Gesser, B., Maare, H., Deleuran, M., Larsen, C., and Thestrup-Pedersen, K. (1995). Regulation of human T lymphocyte chemotaxis in vitro by T cell-derived cytokines IL-2, IFN-gamma, IL-4, IL-10, and IL-13. J. Immunol. *154*, 3742–3752.

Urdzíková, L., Růžička, J., LaBagnara, M., Kárová, K., Kubinová, Š., Jiráková, K., Murali, R., Syková, E., Jhanwar-Uniyal, M., and Jendelová, P. (2014). Human mesenchymal stem cells modulate inflammatory cytokines after spinal cord injury in rat. Int. J. Mol. Sci. *15*, 11275–11293.

Van Dyken, S.J., and Locksley, R.M. (2013). Interleukin-4- and interleukin-13-mediated alternatively activated macrophages: roles in homeostasis and disease. Annu. Rev. Immunol. *31*, 317–343.

Vangansewinkel, T., Geurts, N., Quanten, K., Nelissen, S., Lemmens, S., Geboes, L., Dooley, D., Vidal, P.M., Pejler, G., and Hendrix, S. (2016). Mast cells promote scar remodeling and functional recovery after spinal cord injury via mouse mast cell protease 6. FASEB J. *30*, 2040–2057.

Vidal, P.M., Lemmens, E., Avila, A., Vangansewinkel, T., Chalaris, A., Rose-John, S., and Hendrix, S. (2013). ADAM17 is a survival factor for microglial cells in vitro and in vivo after spinal cord injury in mice. Cell Death Dis. *4*, e954.

Yamasaki, R., Lu, H., Butovsky, O., Ohno, N., Rietsch, A.M., Cialic, R., Wu, P.M., Doykan, C.E., Lin, J., Cotleur, A.C., et al. (2014). Differential roles of microglia and monocytes in the inflamed central nervous system. J. Exp. Med. *211*, 1533–1549.

Yang, M.-S., Ji, K.-A., Jeon, S.-B., Jin, B.-K., Kim, S.U., Jou, I., and Joe, E. (2006). Interleukin-13 enhances Cyclooxygenase-2 expression in activated rat brain microglia: implications for death of activated microglia. J. Immunol. *177*, 1323–1329.